Ruthenium Carbonyl 1,4-Diaza-1,3-butadiene (R-DAB) Complexes. A Theoretical and Experimental Investigation of the Electronic Structure of $Ru_2(CO)_4$(R-DAB)(μ-CO) and $Ru_2(CO)_4$(R-DAB)(μ-HC≡CH)

Maurizio Casarin,*[1a,d] Andrea Vittadini,[1a] Kees Vrieze,*[1b] Fred Muller,[1b] Gaetano Granozzi,*[1c] and Renzo Bertoncello[1c]

Contribution from Istituto di Chimica e Tecnologia dei Radioelementi del CNR, Padova, Italy, Istituto di Chimica, Università della Basilicata, Potenza, Italy, Anorganisch Chemisch Laboratorium, University of Amsterdam, Amsterdam, The Netherlands, and Dipartimento di Chimica Inorganica, Metallorganica ed Analitica, Università di Padova, Padova, Italy.
Received July 6, 1987

Abstract: The electronic structure of two binuclear ruthenium clusters containing the 8e donor 1,4-diaza-1,3-butadiene (R-DAB) ligand [$Ru_2(CO)_4$(R-DAB)(μ-CO) and $Ru_2(CO)_4$(R-DAB)(μ-HC≡CH)] is for the first time discussed by using SCF first principle discrete variational (DV) Xα calculations and gas-phase UV photoelectron (PE) spectroscopy. Despite the short metal–metal interatomic distance, the bonding scheme of both molecules is dominated by the absence of any direct metal–metal bond. On the contrary, the importance of a strong multicentered interaction involving the μ-bridged ligands has been emphasized. As far as the R-DAB moiety is concerned, theoretical results indicated a poorer involvement of n^+ and n^- linear combinations of nitrogen lone pairs than π_3* and π_2 levels in metals–R-DAB interactions. Looking into the nature of such a π interaction it has been found that the Ru atom of the metallacycle fragment is mostly involved in M → π_3* back-bonding while π_2 → M donation mainly involves the second Ru atom.

In the recent past much attention has been devoted to the coordinating capability of α-diimine ligands and to the chemical, spectroscopic, and photochemical properties of their low-valent metal complexes.[2,3] The versatile coordination behavior of substituted 1,4-diaza-1,3-butadiene (RN_α=C_βH—C_βH=N_αR, hereafter R-DAB), which not only acts as a 2e (σ-N)[2a] or 4e (σ-N, σ-N′ chelating)[2a] donor, but also shows 4e (η^2-CN, η^2-CN′),[3b] 2e,2e (σ-N,σ-N′ bridging),[2a] 6e (σ-N, μ_2-N′, η^2-CN′),[2a] and 8e (σ-N, σ-N′,η^2-CN, η^2-CN′)[2a] coordination behavior, is well known. However, in spite of the vast amount of work devoted to the investigation of coordinative, structural, and electronic properties of those complexes where R-DAB acts as a 2e, 4e, and 6e donor,[2,3] no attempt to investigate the electronic structure of organometallic compounds containing the 8e donor R-DAB ligand has been so far reported.

In this paper we report the first combined theoretical and experimental investigation, by means of SCF first principle discrete variational (DV) Xα calculations and gas-phase UV photoelectron (PE) spectroscopy, of the electronic structure of ruthenium binuclear complexes containing the 8e donor R-DAB ligand: $Ru_2(CO)_4$(R-DAB)(μ-CO) (I) and $Ru_2(CO)_4$(R-DAB)(μ-HC≡CH) (II) (R = neopentyl, I; isopropyl, II) (see Figure 1). The main goal of this study is the analysis of the bonding scheme of I and II with particular emphasis on the metal–metal (M–M) and M–ligand interactions. Moreover, it is also interesting to compare the acceptor/donor properties of R-DAB, C_4H_4,[4a,b] and N_4H_2[4c,d] moieties in complexes containing the metallacycle fragment.

Theoretical data are in excellent agreement with the UV–PE experimental results for both molecules, enabling us to accept with confidence the description of the relative bonding schemes dominated by the absence of any direct M–M interaction. To reduce the difficulty in analyzing complex molecular orbital diagrams for the title molecules, we have made use of a density of states (DOS) analysis. Finally, contour plots (CPs) of some molecular orbitals (MOs), particular important for describing metal–metal and metal–ligand interactions, are reported and discussed.

Experimental Section

Spectra. He I and He II excited PE spectra were measured on a Perkin-Elmer PS-18 spectrometer modified for He II measurements by inclusion of a hollow cathode discharge lamp giving high output of He II photons (Helectros Developments). The spectrometer was connected on line with a MINC-23 computer (Digital) by an interface built in our laboratory. Data acquisition was carried out by several sweeps (5–10) over 500 distinct channels. Typical sweep times were 5–10 min. The ionization energy (IE) scale was calibrated by reference to peaks due to admitted inert gases (Xe–Ar) and to the He 1-s^{-1} self-ionization. A heated inlet probe system was adopted at 100–110 °C.

Synthesis. The title compounds were synthesized according to published procedures.[2c,g] After crystallization, their purity was checked by IR and ^{1}H NMR instruments, respectively.

Theoretical Method. SCF Hartree–Fock–Slater (HFS) discrete variational (DV) Xα calculations[5] of I and II were performed on a VAX-11/750 computer at the computing center of the Institute of Chemistry

(1) (a) CNR. (b) University of Amsterdam. (c) Università di Padova. (d) Università della Basilicata.

(2) (a) A recent review dealing with the chemistry of α-diimine ligands is: Vrieze, K. *J. Organomet. Chem.* **1986**, *300*, 307 and references therein. (b) Staal, L. H.; Polm, L. H.; Vrieze, K.; Ploeger, F.; Stam, C. H. *Ibid.* **1980**, *199*, C13. (c) Staal, L. H.; van Koten, G.; Vrieze, K.; Ploeger, F.; Stam, C. H. *Inorg. Chem.* **1981**, *20*, 1830. (d) Staal, L. H.; Polm, L. H.; Vrieze, K.; Ploeger, F.; Stam, C. H. *Ibid.* **1981**, *20*, 3590. (e) Staal, L. H.; van Koten, G.; Vrieze, K.; van Santen, B.; Stam, C. H. *Ibid.* **1981**, *20*, 3598. (f) Staal, L. H.; Keijsper, J.; van Koten, G.; Vrieze, K.; Cras, J. A.; Bosman, W. P. *Ibid.* **1981**, *20*, 555. (g) Keijsper, J.; Polm, L.; van Koten, G.; Vrieze, K.; Abbel, G.; Stam, C. H. *Ibid.* **1984**, *23*, 2142. (h) Polm, L. H.; van Koten, G.; Elsevier, C. J.; Vrieze, K.; van Santen, B. F. K.; Stam, C. H. *J. Organomet. Chem.* **1986**, *304*, 353. (i) Shi, Q.-Z.; Richmond, T. G.; Trogler, W. C.; Basolo, F. *Organometallics* **1982**, *1*, 1033. (j) Gross, M. E.; Ibers, J. A.; Trogler, W. C. *Ibid.* **1982**, *1*, 530. (k) Frühauf, H.-W.; Seils, F. *J. Organomet. Chem.* **1986**, *302*, 59. (l) Brockmann, M.; tom Dieck, H. *Ibid.* **1986**, *314*, 75.

(3) (a) Staal, L. H.; Stufkens, D. J.; Oskam, A. *Inorg. Chim. Acta* **1978**, *26*, 255. (b) Kokkes, M. W.; Stufkens, D. J.; Oskam, A. *J. Chem. Soc., Dalton Trans.* **1984**, 1005. (c) Andrēa, R. R.; Louwen, J. N.; Kokkes, M. W.; Stufkens, D. J.; Oskam, A. *J. Organomet. Chem.* **1985**, *281*, 273. (d) Andrēa, R. R.; De Jager, H. E.; Stufkens, D. J.; Oskam, A. *Ibid.* **1986**, *316*, C24. (e) Kokkes, M. W.; Stufkens, D. J.; Oskam, A. *Inorg. Chem.* **1985**, *24*, 4411 and references therein reported.

(4) (a) Casarin, M.; Ajō, D.; Vittadini, A.; Ellis, D. E.; Granozzi, G.; Bertoncello, R.; Osella, D. *Inorg. Chem.* **1987**, *26*, 2041. (b) Casarin, M.; Ajō, D.; Granozzi, G.; Tondello, E.; Aime, S. *Ibid.* **1985**, *24*, 1241. (c) Trogler, W. C.; Curtis, E. J.; Ellis, D. E. *Ibid.* **1981**, *20*, 980 and references therein. (d) Gross, M. E.; Trogler, W. C.; Ibers, J. A. *J. Am. Chem. Soc.* **1981**, *103*, 192. (e) Thorn, D. L.; Hoffmann, R. *Nouv. J. Chim.* **1979**, *3*, 39. (f) Thorn, D. L.; Hoffmann, R. *Inorg. Chem.* **1978**, *17*, 126.

(5) (a) Averill, F. W.; Ellis, D. E. *J. Chem. Phys.* **1973**, *59*, 6412. (b) Rosen, A.; Ellis, D. E.; Adachi, H.; Averill, F. W. *Ibid.* **1976**, *65*, 3629 and references therein. (c) Trogler, W. C.; Ellis, D. E.; Berkowitz, J. *J. Am. Chem. Soc.* **1979**, *101*, 5896.

0002-7863/88/1510-1775$01.50/0 © 1988 American Chemical Society

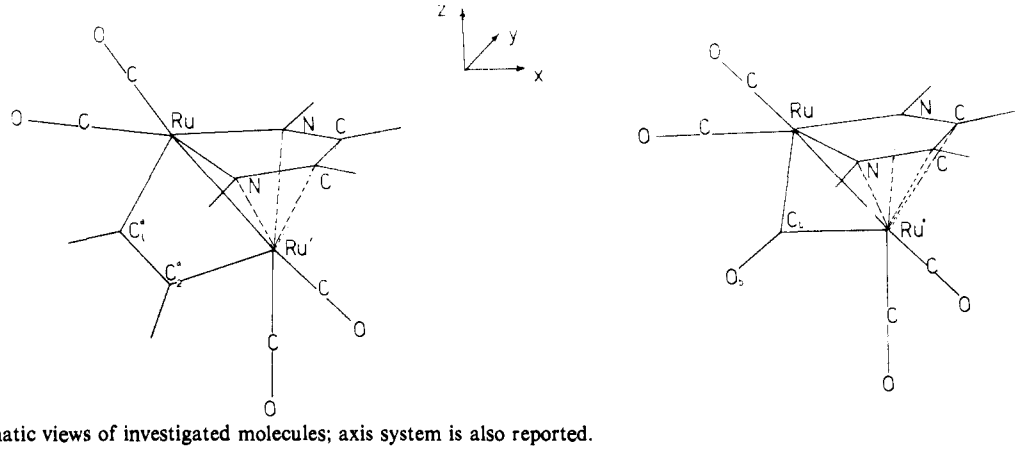

Figure 1. Schematic views of investigated molecules; axis system is also reported.

Table I. Atomic Character from the SCC DV-Xα Calculation of $Ru_2(\mu\text{-CO})(CO)_4$(Me-DAB) (I)

eigenvalue			population, %							
MO	$-E$ (eV)	TSIE	Ru	Ru'	$(CO)_b$	$2(CH)_{DAB}$	2N	$2(CH_3)$	4(CO)	character[b]
30a'[a]	2.53		21	21	8	10	22	4	14	
29a'	4.85	7.20	35	5	9	9	24	3	15	$M \rightarrow \pi_3^*$
28a'	5.61	8.09	26	29	19	4	5	1	16	$(M\text{-}M')^{ab} + \pi_\parallel^*$
21a''	5.75	8.19	44	22	1	3	14	2	14	
27a'	6.34	8.71	12	54	8	5	2	1	18	
26a'	6.52	9.11	62	7	0	2	1	1	27	4d pairs
20a''	6.91	9.38	27	42	12	1	8	1	9	
25a'	7.01	9.52	5	56	0	3	8	3	25	
24a'	7.36	9.81	40	21	3	3	13	3	17	
19a''	7.99	10.32	4	14	0	19	40	12	11	π_2
18a''	8.50	10.82	4	2	4	5	51	15	19	n^-
23a'	9.30	11.60	6	6	2	7	44	12	23	n^+

[a] Lowest occupied MO. [b] ab = antibonding.

and Technology of Radioelements of the CNR.

The approximations of the reported theoretical calculations are: (i) use of near-minimal atomic orbitals (AOs) basis sets; (ii) SCC approximation of Coulomb potential, representing atoms by overlapping spherical charge distributions;[5b] (iii) use of the Gaspar–Kohn–Sham exchange potential;[6] (iv) neglect of correlation terms; (v) neglect of relativistic effects; and (vi) Slater's transition state (TS) formalism[7] to calculate the ionization energies (IEs).

Numerical AOs (through 5p on Ru, 2p on C, N, O, and 1s on H) obtained for the neutral atoms were used as basis functions. Because of the size of the investigated systems, orbitals 1s–4p (Ru) and 1s on carbon, nitrogen, and oxygen were treated as a part of a frozen core in the molecular calculations. Gross atomic charges and bond overlap populations (OPs) were computed using the Mulliken's scheme.[8]

Experimental geometries[2b,c,g] of I and II were idealized to C_s symmetry for use in the calculations (see Figure 1). In order to save computer time, the electronic properties of the R-DAB substituents (R = neopentyl, I; isopropyl, II) have been simulated in both cases by replacing the actual R with a methyl group. The MOs have been then labeled according to the irreducible representations a' and a''.[9] Instead of displaying eigenvalues along an energy axis, the density of states (hereafter DOS) has been plotted as a function of energy. The component, or partial, density of states function (PDOS) for atomic basis function j is constructed according to published procedure.[10] These plots have an advantage over molecular energy level schemes because they provide insight into the disposition and composition of orbitals over a broad range of energy.

(6) (a) Gaspar, R. *Acta Phys. Acad. Sci. Hung.* **1954**, *3*, 263. (b) Kohn, W.; Sham, L. J. *Phys. Rev. A* **1965**, *140*, 1133.

(7) Slater, J. C. *Quantum Theory of Molecules and Solids. The Self-Consistent Field For Molecules and Solids*; McGraw-Hill: New York, 1974; Vol. 4.

(8) Mulliken, R. S. *J. Chem. Phys.* **1955**, *23*, 1833.

(9) The outermost filled μ-bridged ligand MOs transform as a' [I (5σ)] and a' + a'' [II ($\pi_\parallel$ and $\pi_\perp$)] irreducible representations of the C_s symmetry point group pertaining to the whole molecular system (see Figure 1) where $\perp$ and $\parallel$ symbols refer to the plane passing through metal atoms and bridging ligands. Moreover, the a' and a'' MO labeling allows us to distinguish π_3^* and/or π_1 (both a' in symmetry) from π_2 (a'') involvement in the metal–(R-DAB) interaction.

(10) Holland, G. F.; Ellis, D. E.; Trogler, W. C. *J. Am. Chem. Soc.* **1986**, *108*, 1884.

Results and Discussion

A rough description of the bonding scheme of the title molecules can be obtained by partitioning the whole molecular systems into three interacting fragments: $Ru_2(CO)_4$, μ-bridging ligands [CO (I), HC≡CH (II)], and R-DAB. A qualitative description of the $Ru_2(CO)_4$ frontier MOs mainly interacting with the bridging ligand ones can be obtained by making reference to the qualitative extended Hückel (EH) investigation carried out by Hoffman and Hoffmann on the electronic structure of the $Pt_2(CO)_4$ fragment.[11] In the present case, the outermost occupied levels are grouped in a single "block" of eight MOs, consisting essentially of the in-phase and out-of-phase linear combinations of the $M(CO)_2$ orbitals,[11] at variance with the well-known separation into six t_{2g}- and four e_g-like MOs of the $M_2(CO)_6$ fragment.[4e,f] The energy position of the d "block" favors strong interaction with the occupied levels of the μ-bridging ligands [5σ (I) and $\pi_\parallel$ and $\pi_\perp$ (II)][12] lying in the same energy region.[12] These interactions give rise to one (a' in symmetry in I) and two (a' and a'' in II) high-lying MOs having an antibonding metal–ligand character.

With regard to the R-DAB ligand, eight electrons are here available for coordination: two lone pairs on the imine nitrogen atoms (namely, n^+ and n^-) and two pairs of π electrons (π_1 and π_2) on the $N_\alpha{=}C_\beta{-}C_\beta{=}N_\alpha$ skeleton. Moreover, with reference to N_4H_2[4c,d] and C_4H_4[4a,b,e,f] ligands, a third low-lying empty MO (π_3^*)[9] (capable of accepting charge from M atoms through back-donation) is available. On qualitative grounds we expect that the a'-type outermost MO of I and II will be that most involved into the back-bonding interaction with the π_3^* MO.

$Ru_2(CO)_4$(R-DAB)(μ-CO). In Table I the DV-Xα ground-state charge density analysis of the outermost MOs of I is reported. The theoretical results confirm as a whole the aforesaid qualitative bonding scheme. The HOMO (29a'), well distinct in energy from

(11) Hoffman, D. M.; Hoffmann, R. *J. Chem. Soc., Dalton Trans.* **1982**, 1471.

(12) Hoffman, D. M.; Hoffmann, R.; Fisel, C. R. *J. Am. Chem. Soc.* **1982**, *104*, 3858.

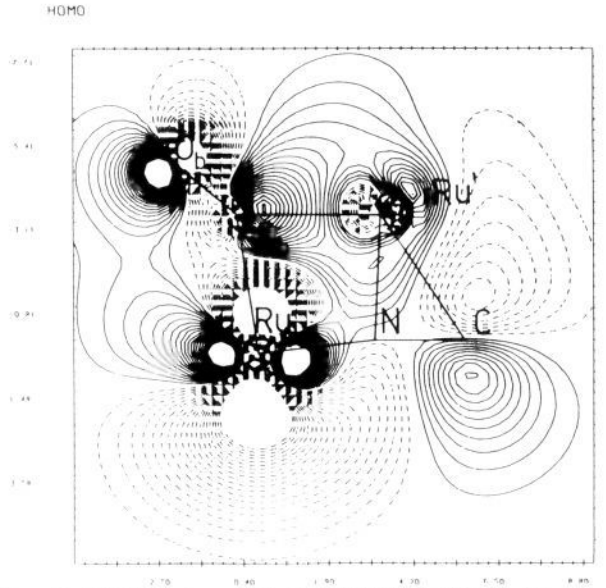

Figure 2. DV–Xα contour plot for the 29a′ HOMO of I in the *XZ* plane. The interval between successive contour levels is 0.0337 $e^{1/2}/Å^{3/2}$.

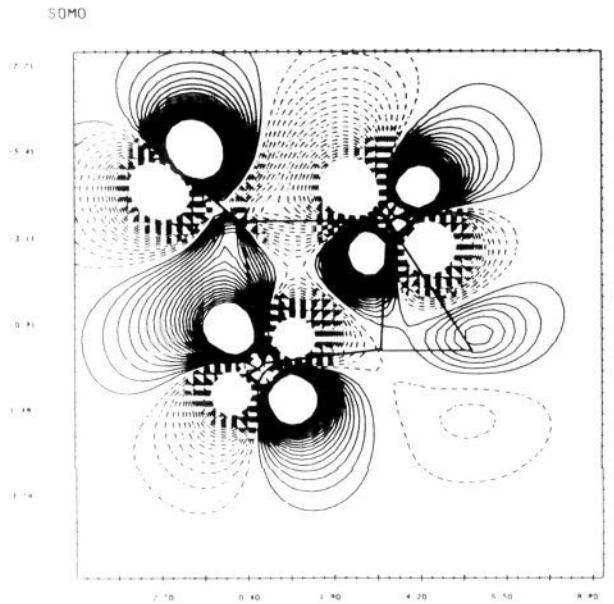

Figure 3. DV–Xα contour plot for the 28a′ SOMO in the *XZ* plane for I. Plot parameters are identical with those of Figure 2.

the subsequent MOs, is delocalized over the whole molecule (see Table I and Figure 2). The contribution to this MO from metal atoms (40%) indicates that it comes from the above-described *d* "block" of $M_2(CO)_4$, while its energy position is a balance of two opposite effects, namely, the destabilizing interaction with the occupied 5σ level of the μ-CO ligand[13] and the stabilizing back-bonding into the π_3* level of R-DAB. Among the remaining seven MOs, belonging to the *d* "block" of $M_2(CO)_4$ (28a′–24a′ in Table I), noteworthy is the nature of the 28a′ SOMO (second occupied molecular orbital) (Figure 3) which is strongly involved into the back-bonding (Ru,Ru′) → $2\pi_{\parallel}$* (μ-CO) orbital.[13]

At lower energy we have levels mainly localized on the ligands. In Table I we decided to report only the outermost occupied ligand based MOs (π_2, n^-, n^+) because the π_1 and 5σ states of R-DAB and μ-CO, respectively, lie at lower energies. In order to identify

(13) We must note that in the whole molecular system 5σ and $2\pi_{\parallel}$* levels of the μ-CO belong to the same irreducible representation (a′) so that they are allowed to mix with each other. Nevertheless, back-bonding into the $2\pi_{\parallel}$* level is mostly accounted for by the 28a′ MO (see Figure 3).

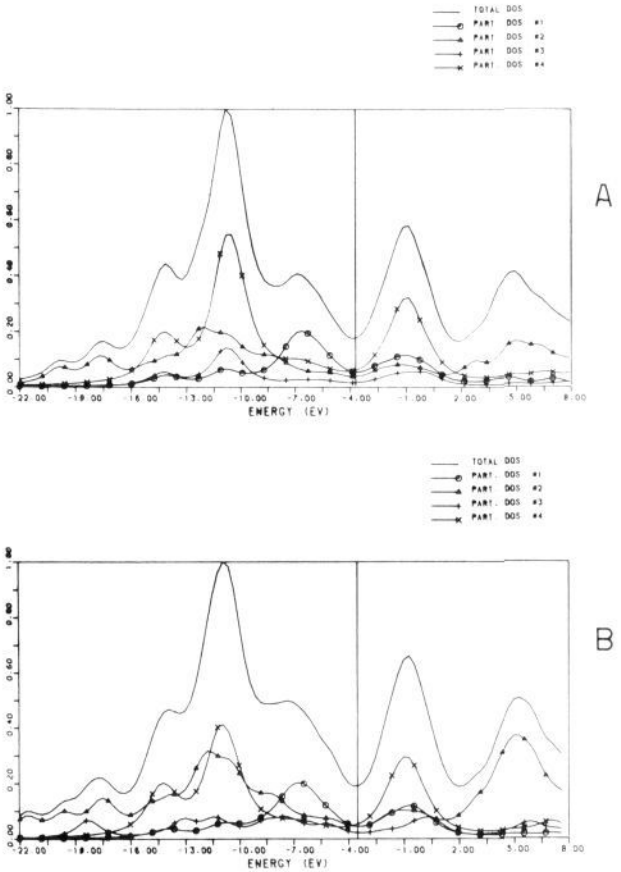

Figure 4. (A) Total and partial density of states for I. (B) Total and partial density of states for II. PDOS are scaled to total DOS: PDOS #1, metal atoms; #2, R-DAB; #3, μ-ligand; #4, terminal carbonyls. Note that since a 0.4-eV Lorentzian broadening factor was used in constructing the DOS plots, regions where there are no orbitals appear as minima, rather than zero.

the energy position of inner ligand based levels, it is useful to refer to PDOS (see Figure 4A) where contributions from metal atoms, terminal carbonyls, R-DAB, and μ-CO are reported.

The scarce metal localization percentage in n^- and n^+ (18a″ and 23a′ MOs, respectively) is noteworthy (see Table I). This result, coupled with the strong localization of the HOMO on the nitrogen pπ AOs, indicates that in I the M–(R-DAB) interaction is mainly π in character. Looking into such an interaction, it is of value to stress that the Ru atom is the mostly involved in the M → π_3* back-bonding while π_2 → M donation mainly involves the Ru′ atom (see Table I).

A deeper insight into the electronic structure of I can be obtained by making reference to Mulliken's gross atomic charges and bond overlap populations (OPs) (see Figure 5A). It is also useful to compare the present results with those pertinent to the isoelectronic $Ru_2(CO)_6C_4H_4$,[14] recently investigated by the authors by using the same theoretical approach.[4a] Both π_2 → M and M → π_3* interactions concur to the R-DAB N_α–C_β bond lengthening and C_β–C_β bond shortening on going from the free ligand to the (σ-N, σ-N′, η^2-CN, η^2-CN′) coordinated one.[15] The strength of the π_2 → M interaction is roughly similar in I and $Ru_2(CO)_6C_4H_4$[19] so that only a stronger M → π_3* interaction in I than in

(14) In the binuclear ruthenacyclopentadienyl derivative, recently investigated,[4a] the fragment C_α=C_β—C_β=C_α exists isostructural with N_α=C_β—C_β=N_α.

(15) In the N_α=C_β—C_β=N_α unit of I, the N_α–C_β (C_β–C_β) bond distance passes from 1.258 Å (1.457 Å)[16] to 1.42 Å (1.40 Å)[2g] on going from the free ligand to the coordinated one. In the corresponding fragment C_α=C_β—C_β=C_α of $Ru_2(CO)_6C_4H_4$, the C_α–C_β (C_β–C_β) bond length passes from 1.34 Å (1.48 Å)[17] (uncoordinated) to ≈1.41 Å (1.41 Å)[18] (coordinated).

(16) Keijsper, J.; van der Poel, H.; Polm, L. H.; van Koten, G.; Vrieze, K.; Seignette, P. F. A. B.; Varenhorst, R.; Stam, C. H. *Polyhedron* **1983**, *2*, 1111.

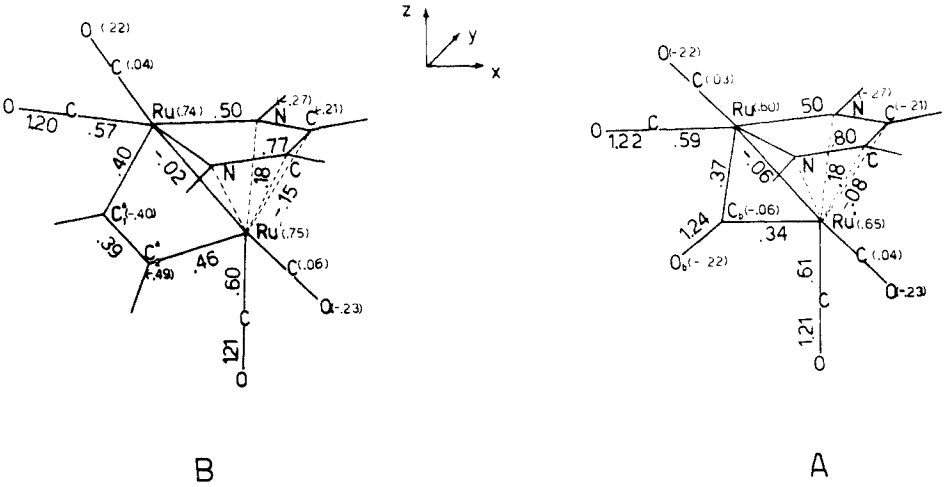

Figure 5. (A) DV-Xα gross atomic charges (in parentheses) and overlap populations of I. (B) DV-Xα gross atomic charges (in parentheses) and overlap populations of II.

Table II. Ionization Energy Data (eV) for the Compounds I and II[a]

band	I	II
(S)A	6.87	(7.24)7.44
B	8.00	8.30
(S)C	(8.78)9.19	(8.87)9.26
(D')D	(11.3)14.0	10.00
E		10.41
(F')(F'')F		(11.3)(12.3)14.4

[a] Shoulders in parentheses.

$Ru_2(CO)_6C_4H_4$ can explain the different bond-length variations on going from the free ligand to the coordinated one.[15] This is in agreement with the smaller R-DAB N_α–C_β OP (0.80 e, Figure 5A) versus the C_4H_4 C_α–C_β one (0.94 e).[4a] Quite unexpectedly, on the basis of the above-described M–(R-DAB) π interactions, Ru and Ru' have the same gross atomic charges. In the present case the Ru–Ru' interaction cannot be invoked as a metal charge balancing mechanism (as in $Ru_2(CO)_6C_4H_4$)[4a] because, despite the short Ru–Ru' interatomic distance (2.741 Å),[2g] the total Ru–Ru' OP is nearly equal to zero (see Figure 5A). Such behavior can be explained only by a very strong multicentered interaction (as eventually computed) between metal atoms and the μ-bridged CO ligand. The high electron density on C_b (compare the gross atomic charges of C_b with those of terminal carbonyls in Figure 5A) indicates that the leading role, in determining the charge balancing between metal atoms, is certainly played by the bridging carbonyl.

The He I/He II excited PE spectra of I, with bands alphabetically labeled, are reported in Figure 6. Relative IE values are reported in Table II. At least three well-resolved bands (A, B, and C) are present in the lower IE region (up to $\approx$10.5 eV). With reference to other polynuclear carbonyl clusters,[20] it is well known that the spectral region beyond this value (the broad band envelope D) includes ionizations from levels primarily localized on the carbonyl groups (5σ, 4σ, and 1π MOs) and from the σ framework of the organic portion of the cluster. In particular, the shoulder D' can be partially related to σ ionizations from the two neopentyl groups of the R-DAB (note the dramatic decrease of D' on passing from the He I to the He II ionization source).[21]

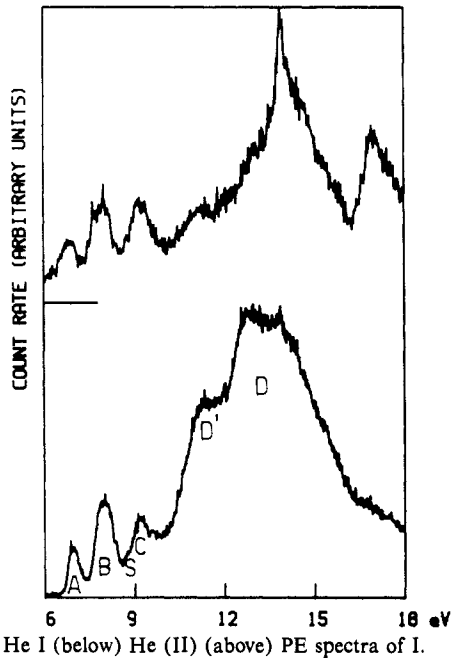

Figure 6. He I (below) He (II) (above) PE spectra of I.

Since a further analysis of this region is not productive, we shall confine ourselves to the discussion of the lower IE region.

With regard to the TSIE results[23] and to intensity arguments (see Table I and Figure 6), band A is assigned to the ionization from the HOMO 29a'. The following band B has to be associated with three ionization events (28a', 21a'', 27a'). Its high He I intensity can be explained by looking at the significant contribution of carbonyls and R-DAB ligand to 28a' and 21a'' MOs.[24] Finally the evident increase under He II radiation of band C (and its shoulder S) (see Figure 6) allows us to assign them as a whole to the ionization from metal-based 26a', 20a'', 25a', and 24a' MOs in agreement with TSIE results. The ionizations from the R-DAB outermost MOs reported in Table I are supposed to be hidden under the shoulder D', so that we cannot compare the IEs of these levels with those relative to mononuclear compounds.[3c]

$Ru_2(CO)_4$(R-DAB)(μ-HC$\equiv$CH). In Table III the DV-Xα ground-state charge density analysis of the outermost MOs of II is reported. As already found in I, quantitative theoretical results confirm the qualitative predictions. In particular, two high-lying MOs (29a' and 21a''), well distinct in energy from the inner ones, are evident (see Table III). The 29a' HOMOs of II and I have

(17) Almenningen, A.; Bastiansen, O.; Traettenberg, M. *Acta Chem. Scand.* **1958**, *12*, 1221.

(18) Noda, I.; Yasuda, H.; Nakamura, A. *J. Organomet. Chem.* **1983**, *250*, 447.

(19) The Ru'–N_a (Ru'–C_a) overlap population of symmetry a'' is the same (0.10 e) in both cases.

(20) Granozzi, G.; Tondello, E.; Casarin, M.; Aime, S.; Osella, D. *Organometallics* **1983**, *2*, 430 and references therein.

(21) In fact, on the basis of the Gelius model,[22a] we expect a marked decrease in the cross-section ratio σ(C 2p)/σ(M nd) on passing from the He I to the He II excitation source.[22b]

(22) (a) Gelius, U. In *Electron Spectroscopy*; Shirley, D. A., Ed.; North Holland: Amsterdam, 1972; p 311. (b) Rabalais, J. W. In *Principles of UV Photoelectron Spectroscopy*; Wiley–Interscience: New York, 1977.

(23) Slater's transition-state calculations[7] have been performed for each MO reported in Tables I and III.

(24) The σ(C, N 2p) cross section is higher than the σ(M nd) one under He I radiation.[22]

Table III. Atomic Character from the SCC DV-Xα Calculation of $Ru_2(\mu\text{-}HC{\equiv}CH)(CO)_4$(Me-DAB) (II)

MO	eigenvalue		population, %							character[b]
	$-E$ (eV)	TSIE	Ru	Ru′	C_2H_2	$2(CH)_{DAB}$	2N	$2(CH_3)$	4(CO)	
30a′[a]	2.11		37	3	19	4	14	2	21	
29a′	4.86	7.15	26	6	6	10	31	4	17	$M \rightarrow \pi_3^*$
21a″	5.09	7.63	28	12	50	2	2	0	6	$(M\text{–}M')^b + \pi_\perp$
20a″	5.84	8.17	27	29	8	3	16	3	14	
28a′	6.16	8.52	13	47	7	10	2	0	21	
27a′	6.45	8.94	58	5	6	2	4	2	23	4d pairs
26a′	6.83	9.24	17	49	4	2	3	2	23	
25a′	7.12	9.55	32	32	6	2	6	2	20	
24a′	7.29	9.74	23	25	41	1	4	1	5	$M,M' \rightarrow \pi_\parallel^*$
19a″	7.57	9.90	17	26	31	3	8	1	14	$\pi_\perp$
18a″	7.91	10.19	9	10	2	19	37	13	10	π_2
17a″	8.35	10.62	3	7	5	5	46	15	19	n^-
23a′	8.56	11.02	13	10	55	2	8	2	10	$\pi_\parallel$
22a′	9.16	11.40	8	6	5	13	38	13	17	n^+

[a] Lowest occupied MO. [b] b = bonding.

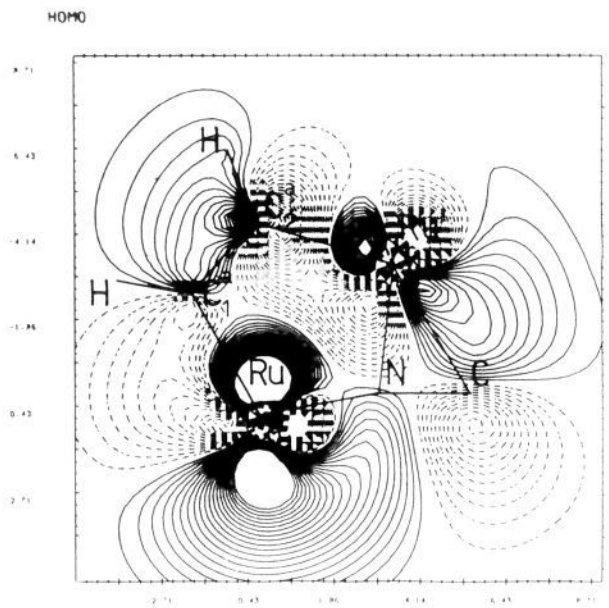

Figure 7. DV–Xα contour plot for the 29a′ HOMO of II in the *XZ* plane. Plot parameters are identical with those of Figure 2.

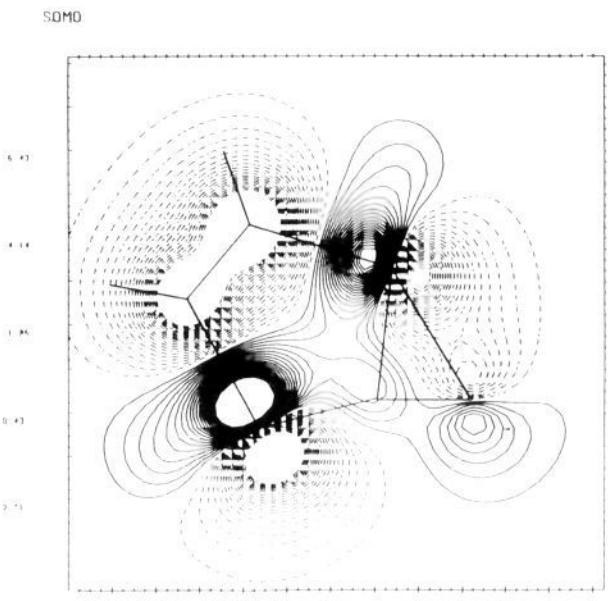

Figure 8. Contour plot for the 21a″ SOMO in the *XZ* plane. The plot represents a slice 1 au above the $Ru_2(\mu\text{-}C_2H_2)$ plane. Plot parameters are identical with those of Figure 2.

a rather similar nature. Actually, in the present case it accounts for the antibonding interaction between metal atoms and the $\pi_\parallel$ orbital of the μ-alkyne and the back-bonding into the R-DAB π_3^* level (Figure 7). Once again the energy position of this MO is a balance of two opposite effects, namely, the destabilizing interaction with the μ-alkyne $\pi_\parallel$ level and the stabilizing back-bonding into the R-DAB π_3^* orbital. The higher localization percentage on the p_π nitrogen AOs in II than in I (see Table III and I) is a consequence of a stronger M–$\pi_\parallel$ (in II) than M–5σ (in I) antibonding interaction. Actually, only by admitting a better energy matching between the highest lying a′ MO of $Ru_2(CO)_4(\mu\text{-ligand})$ and the empty π_3^* level of the R-DAB[9] in II than in I we can explain the increased π acceptor effective capability of the R-DAB ligand in II. Very interesting is the nature of the 21a″ SOMO. This MO (see Figure 8) is Ru–Ru π bonding, and it describes a very strong antibonding interaction between metal atoms and the μ-HC≡CH $\pi_\perp$ level.

Within the remaining six orbitals belonging to the *d* "block", the nature of the 24a′ MO (the innermost of the *d* "block"), which accounts for a very strong $M \rightarrow \pi_\parallel^*$ (see Figure 9) back-bonding interaction, is of relevance. The energy position of this MO, with respect to the 28a′ one in I,[25] is an evident indication of a strong π acceptor capability of μ-HC≡CH compared to the μ-CO. At variance with the bonding scheme already proposed for

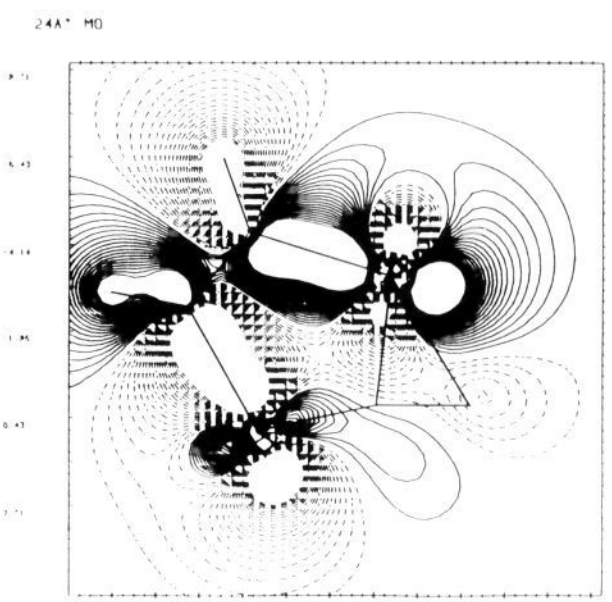

Figure 9. DV–Xα contour plot for the 24a′ MO of II in the *XZ* plane. Plot parameters are identical with those of Figure 2.

(25) The 28a′ MO in I describes the back-bonding interaction from both metals into the $\pi_\parallel^*$ orbital of the μ-CO.

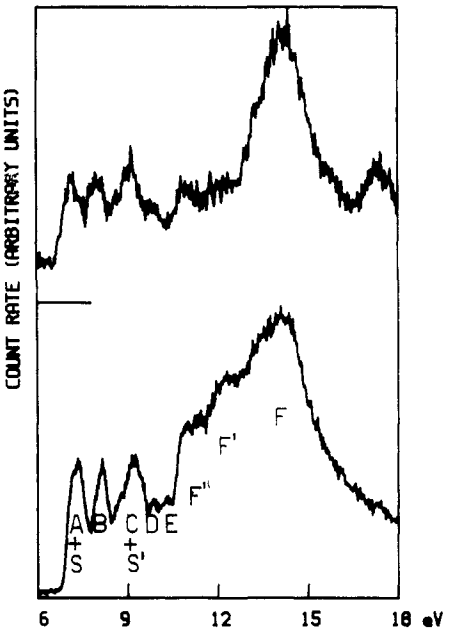

Figure 10. He I (below) He II (above) PE spectra of II.

$(CO)_2M(\mu\text{-}HC{\equiv}CH)M(CO)_2$,[12] where carbonyls were bent away from the parallel alkyne and M → $\pi_\parallel$* (alkyne) was supposed to be poor, in the present case the different coordination geometry of μ-HC≡CH (carbonyls by the same side of the alkyne; see Figure 1) allows a much stronger M → $\pi_\parallel$* interaction.

As already found in I, the Ru–(R-DAB) σ interaction appears to be quite poor compared with the π one. A possible explanation in both cases of this unexpected behavior could be an unfavorable energy matching between n^+, n^-, and suitable $Ru_2(CO)_4(\mu\text{-ligand})$ levels.

As in Table I, only the outermost MOs of the R-DAB ligand have been reported. In order to identify the energy position of inner ligand based levels, one can make reference to Figure 4b where PDOS relative to metal atoms, terminal carbonyls, R-DAB, and μ-HC≡CH are reported. Comparison of A and B in Figure 4 clearly indicates that the gross features of the bonding scheme of both molecules are rather similar.

The gross atomic charges and OPs for II are reported in Figure 5B. First of all the equal Ru′–N OPs in I and II indicate that in both cases the Ru′-(R-DAB) interaction has similar strength; moreover, the ruthenium atoms are more positively charged in II than in I, in agreement with the higher π acceptor capability of μ-HC≡CH versus μ-CO and with the enhanced M → π_3* back-bonding in II. As a final consideration, it is useful to consider the quite scarce $C\text{–}C_{(alk)}$ OP (see Figure 5B), as a consequence of the long $C\text{–}C_{(alk)}$ interatomic distance (1.341).[2b,c] Actually, as in many other alkyne clusters,[26] the parallel-coordinated alkyne undergoes an extensive rehybridization of carbon atoms due to the π and π* orbital involvement in the alkyne–cluster interaction.

Moving on to the discussion of PE experimental results of II (Figure 10, Table II), the proposed bonding schemes nicely match PE spectral pattern variations on going from I to II. Moreover, the less bulky alkyl substituents on R-DAB in II allow detection of two extra bands [bands D and E (see Figure 10)] not seen in the PE spectra of I.

Bands A (with its shoulder S on the lower IE side) and B are both associated with two ionization events: i.e., (S + A) 29a′ HOMO and 21a″ MO; (B) 20a″ and 28a′ MOs. The higher He I intensity of band A with respect to B is ascribed to the large contributions from N and C 2p AOs to 29a′ and 21a″ MOs, respectively (see Table III and Figure 10).[24] This assignment is corroborated by the relative intensity increase of both shoulder S and band B with respect to A under the He II ionizing source.[21,27]

(26) Aime, S.; Bertoncello, R.; Busetti, V.; Gobetto, R.; Granozzi, G.; Osella, D. *Inorg. Chem.* **1986**, *25*, 4004 and references therein.

Band C and its shoulder S′ are associated with confidence to the ionization from four MOs as a whole. On the basis of TSIE results (see Table III), we propose to relate S′ to the ionization from the 27a′ MO and band C to the 26a′–24a′ MOs. This assignment is in line with relative intensity variations shown by this band envelope on passing to more energetic radiation (Figure 10).[21] In particular, the decrease of the higher IE side of band C is in excellent agreement with the large localization percentage (40%) of the 24a′ MO on the C 2p AOs of the μ-bridged ligand.

Bands D and E are both related to a single ionization event, namely, the 19a″ ($\pi_\perp$ alkyne) and 18a″ (π_2 R-DAB) MOs. Even though both bands show a relative intensity decrease under He II radiation[21] (Figure 10), it is noteworthy to point out their different behavior. Actually band E decreases much more than band D (see Figure 10) in agreement with the larger metal contribution 43% of the 19a″ MO versus 19% of the 18a″ one.[20] The IE value of band D (10.00 eV; related to the ionization from $\pi_\perp$) is in agreement with PE findings of many other clusters containing parallel alkynes;[26] on the contrary, it is important to say something more about the IE value of π_2 ionization (10.41 eV). On a qualitative ground we would have expected for the η^2-CN, η^2-CN′ coordinated π_2 level a much higher IE than in the mononuclear σ-N, σ-N′ chelated $Ru(CO)_3$(R-DAB),[3c] where the experimental IE value of the π_2 level lies at IE > 10 eV.[28] The explanation of such behavior is similar to that already invoked to explain the counterintuitive IE values of coordinated olefin π level.[29] Actually, since the R-DAB ligand possesses both donor and acceptor capabilities, the resulting IE value comes out from the balance of two concurrent but opposite terms which tend to cancel each other.

Conclusions

Several conclusions can be drawn from this contribution. Quite counterintuitively with respect to the metal–metal internuclear distance and qualitative electron counting methods,[30] a direct metal–metal bond in both I and II is absent. This apparent worrying point can easily be explained by the well-known flatness of the metal–metal Morse curve[31] and the failure of qualitative theories in the presence of strong back-bonding interactions when one deals with low-valent electron-rich metal atoms.[32] In the present case where two isoelectronic molecules are involved, the actual distance between the ruthenium atoms is determined by the different bite of the bridging CO and HC≡CH. Actually, the Ru–Ru′ distance passes from 2.74 Å in I to 2.94 Å in II even though the Ru′–R–DAB and Ru–N mean distances are very similar [2.27 Å (I), 2.23 Å (II) and 2.14 Å (I), 2.11 Å (II)] in both molecules. The only way to achieve such a result is by pushing the Ru atom out of the DAB plane more in II than in I.[33]

The bonding scheme obtained by theoretical results is also of value for further insights into the reactivity of title molecules. Actually, we have found that reaction of I with CO resulted in

(27) Shoulder S (related to the ionization from the 29a′ HOMO) has a higher localization percentage on *d* metal atoms AOs than b and A, which in turn is associated with the ionization from the 21a″ MO having a 50% localization on C 2p AOs.

(28) The ionization from π_2 level in $Ru(CO)_3$(R-DAB) is hidden under a broad band whose onset is at ≈10 eV.[3c]

(29) Calabro, D. C.; Lichtenberger, D. L. *J. Am. Chem. Soc.* **1981**, *103*, 6846.

(30) Wade, K. *Adv. Inorg. Chem. Radiochem.* **1976**, *18*, 1.

(31) The shallowness of the metal–metal Morse curve points out that, except in extreme cases, the metal–metal internuclear distance is not a good tool to say whether or not a direct interaction between metals is present.

(32) (a) Pinhas, A. R.; Hoffmann, R. *Inorg. Chem.* **1979**, *18*, 654. (b) Mitscher, A.; Rees, B.; Lehmann, M. S. *J. Am. Chem. Soc.* **1978**, *100*, 3390. (c) Bēnard, M. *Ibid.* **1978**, *100*, 7740. (d) Bēnard, M. *Inorg. Chem.* **1979**, *18*, 2782. (e) Granozzi, G.; Tondello, E.; Bēnard, M.; Fragalā, I. *J. Organomet. Chem.* **1980**, *194*, 83. (f) Granozzi, G.; Casarin, M.; Ajò, D.; Osella, D. *J. Chem. Soc., Dalton Trans.* **1982**, 2047. (g) Bottomley, F. *Inorg. Chem.* **1983**, *22*, 2656. (h) Pilloni, G.; Zecchin, S.; Casarin, M.; Granozzi, G. *Organometallics* **1987**, *6*, 597. (i) Schugart, K. A.; Fenske, R. F. *J. Am. Chem. Soc.* **1986**, *108*, 5094.

(33) The dihedral angle between the planes N_α–Ru–N_α and $N_\alpha\text{–}C_\beta\text{–}C_\beta\text{–}N_\alpha$ is 6.5° in I and 14° in II.

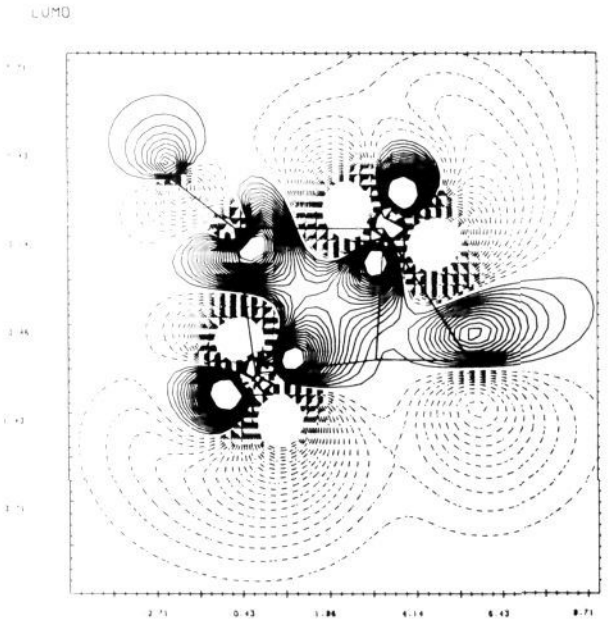

Figure 11. DV–Xα contour plot for the 30a′ LUMO of I in the *XZ* plane. Plot parameters are identical with those of Figure 2.

the formation of $Ru_2(CO)_6$(R-DAB), where the R-DAB is now a σ-N, μ^2-N′, η^2-CN′ 6e donor, and only terminal carbonyls are present.[2g] As yet, no crystal structure of this compound has been obtained but we can assume the presence of a "normal" metal–metal internuclear distance, making reference to X-ray crystal structures of the isoelectronic homo- and heterodinuclear analogues [$Fe_2(CO)_6$(c-Hex-DAB)[34] and $FeRu(CO)_6$(*i*-Pr-DAB)[35]] where the metal–metal distances are 2.597 and 2.660 Å, respectively. This is in agreement with the LUMO (30 a′) nature of I (see Figure 11), which is Ru–Ru′ bonding but strongly antibonding between metals and the bridging CO and R-DAB ligands. The filling up of this MO will destroy the coordination of the bridging CO and will affect the bonding of the R-DAB ligand.

It is also of value to analyze the LUMO nature of II (see Figure 12). This MO (30 a′) (Ru–Ru′ and Ru–C_1^a antibonding but Ru′-C_2^a bonding) is significantly different from the LUMO of I. We are tempted to relate the reactivity and molecular structure (vide infra) of the recently synthesized heterodinuclear cluster [$FeRu(CO)_5$(*i*-Pr-DAB)(μ_2-HC≡CC(O)OMe) (III)][36] to the

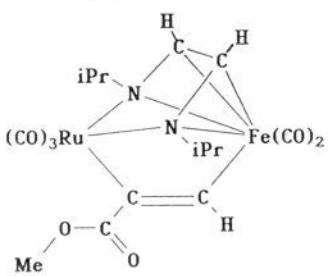

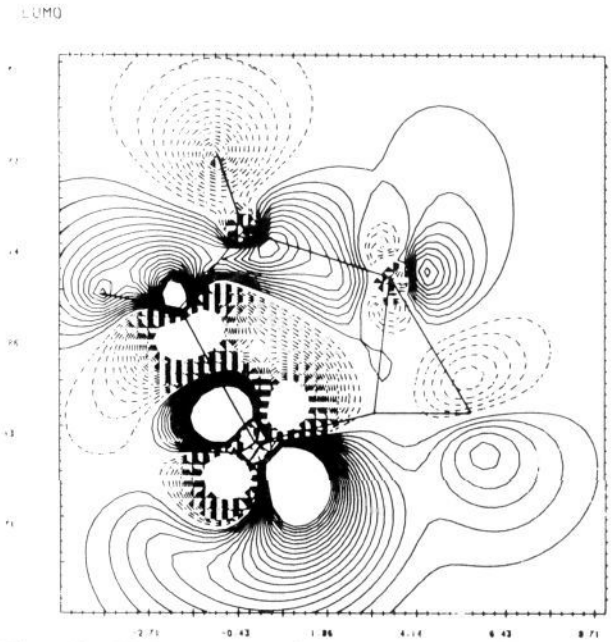

Figure 12. DV–Xα contour plot for the 30a′ LUMO of II in the *XZ* plane. Plot parameters are identical with those of Figure 2.

filling up of a MO similar in nature to the LUMO of II.

The complex III is formed in the reaction of $FeRu(CO)_6$(*i*-Pr-DAB) with methyl propionate at room temperature. The compound easily loses CO when a solution of it is purged with N_2, resulting in the formation of a molecule isostructural with II. The obtained compound reacts with CO to give III again. The crystal structure results of III[36] indicate a longer Ru–C bond length for the third terminal CO with respect to the other terminal CO's on Ru (2.02 Å vs 1.88 Å), which is in agreement with the feasibility of the CO elimination. They also show a nonbonding Fe···Ru distance (3.09 Å), which can be related to the Ru–Ru′ antibonding nature of the LUMO of II.

Finally, as far as complex II, we concluded that μ-HC≡CH is a stronger π acceptor than μ-CO. This could explain the rapid reaction of I in the presence of HC≡CH to give II.[35]

Further conclusions can be inferred from experimental PE results. In contrast with the qualitatively predicted piling of *d* orbitals in a *d* "block", the reported PE data show that *d* ionizations have a resolved structure. Its origin has ultimately to be traced back to the metal–metal and metal–μ-ligand interactions. In both molecules the PE band lying at the lowest IE (band A) contains ionizations from MOs antibonding in nature between metal atoms and the μ-ligand; on the contrary, bands B and C are due to ionizations from M–M antibonding and bonding/nonbonding MOs, respectively.[37]

Acknowledgment. Thanks are due to the CNR of Rome for generous financial support of this study and to Mr. F. De Zuane for invaluable technical assistance.

Registry No. I, 90219-29-7; II, 90219-26-4.

(34) Frühauf, H.-W.; Landers, A.; Goddard, R.; Krüger, C. *Angew. Chem.* **1978**, *90*, 56.

(35) Muller, F.; Vrieze, K.; van Koten, G.; Heijdenrijk, D. *Organometallics*, to be published.

(36) Muller, F.; Kraakman, M.; Vrieze, K.; van Koten, G.; Heijdenrijk, D.; Duineveld, C. A. A.; Stam, C. H., manuscript in preparation.

(37) The nature of the M–M interaction (bonding, antibonding, nonbonding) has been assessed on the basis of the relative CPs.